



# Carbon deposition on Co catalysts during Fischer–Tropsch synthesis: A computational and experimental study

Kong Fei Tan<sup>a</sup>, Jing Xu<sup>a</sup>, Jie Chang<sup>b</sup>, Armando Borgna<sup>b</sup>, Mark Saeys<sup>a,\*</sup>

<sup>a</sup> Department of Chemical and Biomolecular Engineering, National University of Singapore, 4 Engineering Drive 4, Singapore 117576, Singapore

<sup>b</sup> Institute of Chemical and Engineering Sciences, 1 Pesek Road, Singapore 627833, Singapore

## ARTICLE INFO

### Article history:

Received 22 February 2010

Revised 10 May 2010

Accepted 16 June 2010

Available online 27 July 2010

### Keywords:

Fischer–Tropsch Synthesis

Carbon deposition

Deactivation

Graphene

Carbide

## ABSTRACT

The deactivation of a 20 wt% Co/ $\gamma$ -Al<sub>2</sub>O<sub>3</sub> catalyst during Fischer–Tropsch Synthesis (FTS) at 240 °C, 20 bar, and a H<sub>2</sub>:CO ratio of 2 was studied in a fixed-bed micro-reactor. The CO conversion had reduced by 30% after 200 h, and both carbidic and polyaromatic carbon species could be detected on the catalyst using a combination of Temperature-Programmed Hydrogenation (TPH), X-ray Photoelectron Spectroscopy (XPS) and High Resolution Transmission Electron Microscopy (HRTEM). Using Density Functional Theory (DFT), the relative stability of different types of deposited carbon on the Co catalyst was evaluated. Extended layers of graphene were the most stable form, followed by a p4g surface carbide phase initiating from the step edges. Both are more stable than surface CH<sub>2</sub> groups by 99 and 79 kJ/mol. The calculated C 1s core-level binding energies of 284.5 and 283.4 eV further support the presence of polyaromatic carbon and of a surface carbide.

© 2010 Elsevier Inc. All rights reserved.

## 1. Introduction

Fischer–Tropsch Synthesis (FTS) is regaining interest as a process for the production of long-chain hydrocarbons from syngas, a mixture of CO and H<sub>2</sub> [1]. Both Co and Fe are used as FTS catalysts, however, Co catalysts are preferred for gas to liquid (GTL) applications because of the lower water gas shift activity and the higher paraffinic nature of the resulting synthetic crude [2–5]. Supported Co catalysts are known to deactivate during FTS, and the various mechanisms involved have been recently reviewed by Saib et al. [6] and Tsakoumis et al. [7]. In summary, sintering [8,9], oxidation by water [4,8–10] and carbon deposition [11–13] have been proposed. The relative importance of the different mechanisms depends on the catalyst parameters and reaction conditions, as discussed in detail in recent reviews [6,7].

Sintering is reported to be important during the initial rapid deactivation phase [14,15]. Moodley et al. [12] studied the deactivation of supported Co/ $\gamma$ -Al<sub>2</sub>O<sub>3</sub> catalysts in a pilot scale 100 barrel/day slurry bubble column reactor under realistic FTS conditions of 230 °C, 20 bar and a H<sub>2</sub>:CO ratio of 2. Characterization of catalyst samples collected from the reactor showed a gradual build-up of resilient carbon species. In a similar study, Font Freide et al. [13] detected a gradual deposition of carbon on a 20 wt% Co/ZnO

catalyst and attributed the observed deactivation to the deposited carbon. Carbon deposition was also reported for a Ru-promoted Co catalyst [14] and for a 20 wt% Co/SiO<sub>2</sub>-zeolite catalyst [16]. Patents describing techniques to prevent carbon deposition on FTS Co catalysts further illustrate the industrial relevance of this problem [17–19].

Due to the wide range of carbon products present on the catalyst, identifying the nature of the resilient carbon species has proven challenging. Beitel et al. [20,21] observed the formation of a surface cobalt carbide on a model Co(0 0 0 1) surface with X-ray Photoelectron Spectroscopy (XPS) after annealing at 220 °C and 100 mbar in a synthesis gas atmosphere. The surface carbide is believed to form after a CO-induced reconstruction of the Co surface [20]. Using Scanning Tunneling Microscopy (STM), Wilson and de Groot [22] also observed a dramatic reconstruction of the Co(0 0 0 1) surface after exposure to synthesis gas, supporting the formation of a cobalt carbide as observed by Beitel et al. [20,21]. In situ X-ray diffraction (XRD) studies by Ducreux et al. [11] suggest that a bulk cobalt carbide, Co<sub>2</sub>C, gradually forms during FTS at 230 °C, 3 bar and at a high H<sub>2</sub>:CO ratio of 9. The gradual increase in the Co<sub>2</sub>C signal could further be correlated with the decrease in the CO conversion [11]. Based on Temperature-Programmed Hydrogenation (TPH) data, Moodley et al. suggested that resilient polymeric carbon species form gradually on the Co catalyst during FTS [12]. These resilient carbon species reduce the hydrogen uptake in chemisorption experiments [12] and might shift the hydrocarbon selectivity towards more unsaturated products due to the reduced hydrogenation activity of the catalyst [23].

\* Corresponding author. Fax: +65 6779 1936.

E-mail addresses: [armando\\_borgna@ices.a-star.edu.sg](mailto:armando_borgna@ices.a-star.edu.sg) (A. Borgna), [chesm@nus.edu.sg](mailto:chesm@nus.edu.sg) (M. Saeys).

The chemisorption of atomic carbon and graphene on a Co surface has also been studied using Density Functional Theory (DFT) [24–27]. Graphene was calculated to be significantly more stable than isolated surface carbon [24]; hence, the formation of graphene is thermodynamically favorable under FTS conditions. Calculations by Swart et al. [25,26] indicate that graphene overlayers can form directly on the terraces of a Co(1 1 1) catalyst during FTS, as well as nucleate from step sites. The stability of C, O, CO, CH and CH<sub>2</sub> on a Co(1 1 1) surface was studied by Ciobîcă et al. [27]. It was found that surface carbon can induce a reconstruction of the compact Co(1 1 1) surface to the more open Co(1 0 0) surface. These calculations provide support for the experimentally observed surface reconstruction after exposure to syngas or CO [20–22]. Carbon deposition on Ni catalysts has received significantly more attention because of the severe carbon deposition during high-temperature hydrocarbon steam reforming. Several types of deposited carbon have been proposed for Ni. Step and defect sites were identified as nucleation centers for the growth of graphene islands [28–30]. Blocking those sites with trace amounts of S was found to significantly reduce the deactivation rate [31]. More recently, promoters such as Au [29], K [30] and B [32,33] were proposed to enhance the stability of Ni catalysts. Calculations further indicate that the formation of subsurface carbon [32] and of a p4g clock-reconstructed surface carbide [34,35] are feasible under certain conditions. A carbon-induced p4g clock reconstruction was first observed using Low Energy Electron Diffraction (LEED) on a Ni(1 0 0) surface [36]. More recently, a p4g clock reconstruction was found to grow from the step sites on a stepped Ni(1 1 1) surface during decomposition of CO and of ethylene [37,38]. In a p4g clock reconstruction, the surface atoms undergo small displacements, creating a mixture of 4-fold and 3-fold hollow sites. The driving force for this reconstruction is the increased binding energy at the newly created sites.

In this paper, we use DFT to evaluate the binding energy and the thermodynamic stability of different forms of deposited carbon on Co(1 1 1) terraces and near-step sites under FTS conditions. We compare the computational results with characterization data for carbon deposited during realistic FTS. Careful characterization of a 20 wt% Co/γ-Al<sub>2</sub>O<sub>3</sub> catalyst after 200 h on stream indicates the presence of both surface carbide-type carbon and of polyaromatic carbon species. The calculations indicate that large graphene islands are the most stable form of carbon under FTS conditions. However, carbon diffusion into the step sites forming a p4g surface carbide is also highly favorable and preferred over the growth of small graphene islands. Both the experimental and the theoretical results support the formation of two types of resilient carbon during FTS. Finally, the main conclusions are summarized in Section 4.

## 2. Experimental and computational methods

### 2.1. Catalyst synthesis

A γ-Al<sub>2</sub>O<sub>3</sub> support (BET surface area of 380 m<sup>2</sup>/g) was impregnated with an aqueous cobalt nitrate solution (Sigma–Aldrich, 98% purity) to produce Co loadings of 20 wt%. Such Co loadings are typical for commercial applications, and it is generally accepted that deactivation by oxidation is minimized for such loadings and Co particle diameters [6,7,9]. Following impregnation, the slurry was dried at 80 °C under a 80 mbar vacuum in a rotary evaporator (Buchi R-205) with a temperature bath control (Buchi B-490) and kept overnight in an oven at the same temperature. A stationary furnace (Carbolite RWF 1200) was used for calcination. Samples were placed inside large crucibles with a 0.5 cm bed depth to ensure uniform heating. Samples were heated in air to 120 °C at 1 °C/min and kept at 120 °C for 1 h to remove adsorbed moisture.

Thereafter, the samples were heated in air to 400 °C at 1 °C/min and kept at 400 °C for 2 h for calcination. Small amounts of platinum (0.05 wt%, tetra-amine platinum nitrate, Sigma–Aldrich, 99% purity) were added to improve the reducibility of the Co catalyst, as illustrated by Temperature Program Reduction (TPR) profiles and hydrogen uptake data (Fig. 1 and Table 1 in the Supplementary material).

### 2.2. Fischer–Tropsch synthesis

The activity, selectivity and deactivation of the Co catalysts were tested using a fixed-bed micro-reactor equipped with a three-zone heater coupled with independent thermocouples. The reactor has an internal diameter of 2.0 cm and was loaded with 1.0 g of catalyst with a particle size range of 210–300 μm. The catalyst was diluted with approximately 18 g of SiC (1:10 v/v) with the same particle size range to avoid possible temperature gradients. Bed temperatures measured at different depths by moving the thermocouple inside the thermowell indicate that the temperature gradient across the bed is less than 1 °C. During experiments, the temperature in the catalyst bed remained constant. The Weisz–Prater criteria were used to evaluate the possible importance of mass transfer limitations [39]. The calculated Weisz modulus  $\Phi$  of approximately 0.14 for our experimental conditions is lower than the critical value of 1.0, suggesting that no significant mass transfer limitations are expected under our experimental conditions. Catalytic experiments with a larger particle size (300–400 μm) were performed to verify the effects of mass transfer limitations. No appreciable differences in selectivity and conversion were obtained between the larger and smaller particle sizes, further confirming that mass transfer limitations were negligible. The catalyst was reduced in situ for 12 h under H<sub>2</sub> (50 N ml/min, 500 °C and atmospheric pressure) and allowed to cool to 120 °C. Next, syngas with a H<sub>2</sub>:CO ratio of 2.0 was introduced at a W/F of 7.5 g<sub>cat</sub> h/mol (H<sub>2</sub>, Soxal, 99.9%, and a CO/Ar mixture, Soxal, 95:5%), and the reactor was brought to 20 bar and 240 °C with a slow heating rate of 0.5 °C/min. Similar reaction conditions can be found in the literature [40,41]. The catalysts were tested for 200 h, after which the reactor temperature was reduced to 120 °C under flowing synthesis gas, and the catalyst was removed for characterization. The Co catalysts were separated using a magnet, and condensed waxes were extracted using hexane inside a glove box [42]. While solvent extraction under mild conditions may not remove all the waxes, the waxes were removed to very low levels in our experiments as indicated by the TEM and XPS data. Deactivation of Co catalysts during FTS is characterized by a rapid deactivation phase, followed by a slower deactivation phase that governs the long-term deactivation kinetics [14,15]. Both phases were observed in our experiments (Fig. 1), and a 200-h reactor test is considered sufficient to evaluate the kinetics of the slower deactivation phase [43,44]. Products were analyzed online with an Agilent GC 6890 gas chromatograph equipped with a thermal conductivity detector (TCD) and a flame ionization detector (FID). Condensed waxes were analyzed offline with a high-temperature Shimadzu GC 2010 to determine the yields for C<sub>20</sub> to C<sub>80</sub> hydrocarbons. The mass and carbon balance could both be closed to between 95% and 99%.

### 2.3. Catalyst characterization

The catalyst dispersion and particle size were determined from hydrogen adsorption isotherms obtained with a Quantachrome Autosorb 1C. A U-shaped quartz cell was loaded with 0.2 g of the Co/γ-Al<sub>2</sub>O<sub>3</sub> catalyst. First, the samples were heated to 500 °C at a rate of 1 °C/min and reduced in H<sub>2</sub> at 500 °C for 2 h. After reduction, the quartz cell was evacuated at 500 °C for 1 h, before cooling

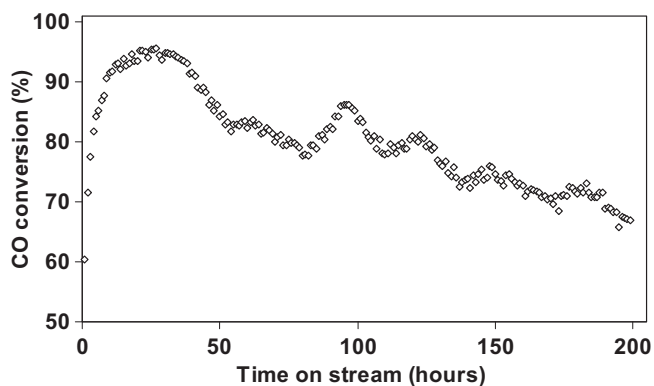


**Fig. 1.** CO conversion as a function time on stream for a 20 wt% Co/ $\gamma$ -Al<sub>2</sub>O<sub>3</sub> FTS catalyst. Reaction conditions: 240 °C, 20 bar, H<sub>2</sub>:CO = 2.0, W/F = 7.5 g<sub>cat</sub> h/mol.

to 25 °C under vacuum. H<sub>2</sub> adsorption isotherms were measured between 80 and 800 mbar at 25 °C. After evacuation for 1 h, a second isotherm was collected to determine strongly and weakly adsorbed hydrogen. The amount of chemisorbed H<sub>2</sub> was determined by extrapolation of the linear part of the isotherm to zero pressure. The particle size and dispersion for the Co catalyst, after reduction at 500 °C is comparable to values reported after reduction at 400 °C [45]. To evaluate the importance of catalyst sintering, the dispersion of the Co catalysts was re-determined after 200 h on stream. After extracting the waxes with hexane, the catalyst samples were hydrogenated at 500 °C in 50 N ml/min for 2 h to remove most of the resilient carbon species, and H<sub>2</sub> chemisorption data were collected following the procedure described earlier. A H:Co ratio of 1 was used to determine the number of surface Co atoms, the dispersion and the turnover frequency (TOF) [46].

The reactivity and the amount of deposited carbon were quantified with TPH and Thermo-Gravimetric Analysis (TGA). About 20 mg of catalyst was loaded in a quartz tube, pretreated with Ar at 200 °C for 1 h to remove weakly adsorbed hydrocarbons, and cooled to room temperature. Next, 50 N ml/h H<sub>2</sub> was introduced and the temperature increased to 600 °C at 5 °C/min. The TPH profile was recorded with a Hiden HPR 20 mass spectrometer operating at a vacuum of 10<sup>-6</sup> Torr or better. The mass spectrometer was calibrated using methane. For the TGA, 20 mg catalyst was placed in a thermobalance basket, again kept under Ar at 200 °C for 1 h and cooled to room temperature. Subsequently, 50 N ml/h H<sub>2</sub> was introduced in the Setaram Setsys Evolution 12 thermobalance, and the relative weight loss profile was recorded until 850 °C at a rate of 20 °C/min.

The nature of the deposited carbon was analyzed by XPS using a Thermo ESCALAB 250 spectrometer equipped with an aluminum anode (Al K $\alpha$  = 1486.6 eV). Measurements were recorded for a

20 eV pass energy, a 0.1 eV kinetic energy step and a 0.1-s dwelling time. Energy corrections were performed using the Al 2p peak of Al<sub>2</sub>O<sub>3</sub> at 74.3 eV. Samples were prepared in a glove box by pulverizing the wax-extracted catalyst. The powders were pressed into an indium layer mounted on a stainless steel XPS stub and transferred from the glove box to the XPS chamber using a method developed for Ni catalysts [33].

High Resolution Transmission Electron Microscopy (HRTEM) images of the Co catalyst after reaction were collected on a Tecnai TF20 microscope at 200 keV. HRTEM samples were prepared by pulverizing the wax-extracted catalyst, followed by sonication at room temperature for 30 min. Samples were then transferred from the glove box to the HRTEM using a method developed for Ni catalysts to minimize exposure to air [33].

#### 2.4. Computational details

Carbon binding energies were computed using periodic spin-polarized DFT with the Perdew–Burke–Ernzerhof (PBE) functional [47] as implemented in the Vienna Ab-initio Simulation Package (VASP) [48,49]. All calculations were performed using the projector-augmented wave method and a plane wave basis with a cutoff energy of 450 eV. Co terraces were modeled with a three-layer fcc Co(1 1 1) slab where the bottom layer was fixed at the bulk positions. Although the hcp structure is preferred for bulk Co, the fcc phase is more stable for crystallites below 100 nm [50]. Step sites were modeled by removing two or four rows of Co atoms from the top layer of a  $p(2 \times 8)$  or  $p(4 \times 8)$  Co(1 1 1) slab (Fig. 2). A similar model has been used to study the formation of a p4g surface carbide on Ni catalysts [34,35]. The optimized bulk lattice constant, 3.52 Å, agrees well with the experimental value of 3.55 Å [51]. To ensure numerical convergence, a  $(5 \times 5 \times 1)$  Monkhorst–Pack  $k$ -point grid was used for  $p(2 \times 2)$  calculations, while a  $(2 \times 2 \times 1)$   $k$ -point grid was sufficient for the  $p(2 \times 8)$  and  $p(4 \times 8)$  unit cells. A vacuum spacing of 10 Å was used to reduce interactions between repeating slabs. Binding energies were found to be converged within 5 kJ/mol with respect to vacuum spacing and  $k$ -point sampling. Increasing the slab thickness to 5 layers decreased the binding energy of carbon and CH groups on the Co terraces by 7 kJ/mol and 5 kJ/mol, respectively, while this increased the binding energy at the p4g clock sites of the stepped surface by 7 kJ/mol.

Binding energies for C, CH and CH<sub>2</sub> species on the terrace and at the step sites were computed using:

$$E_{\text{binding}} = [E_{(X/\text{Co})} - E_{(\text{Co, clean})} - N_X E_{(X)}] / N_X \quad (1)$$

where  $E_{(X/\text{Co})}$ ,  $E_{(\text{Co, clean})}$  and  $E_{(X)}$  represent the total DFT energy for the combined adsorbate/Co system, for the clean surface and for the gas-phase species X, respectively, and  $N_X$  is the number of adsorbates per unit cell. To evaluate the stability of the various species under Fischer–Tropsch conditions, reaction free energies,  $\Delta G_r$ ,

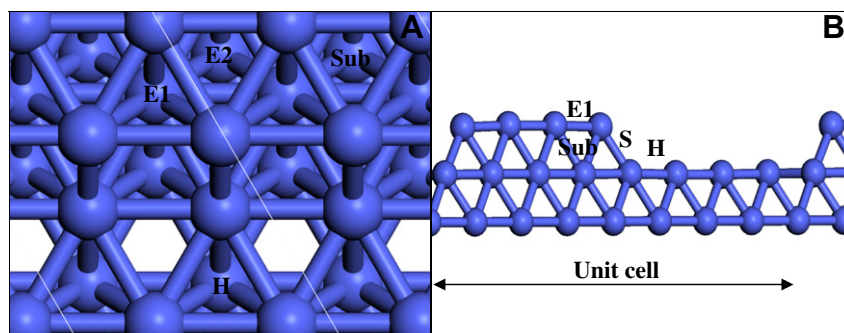
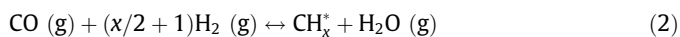


**Fig. 2.** Adsorption sites on a stepped Co surface created by removing four rows of surface Co atoms from a three-layer,  $p(2 \times 8)$  Co(1 1 1) slab. Top (A) and side view (B). S denotes step sites, E1 and E2 are near-step hollow sites, Sub is a subsurface site, and H indicates an hcp hollow site on the lower terrace.

(500 K, 20 bar), with respect to a gas-phase reservoir of CO, H<sub>2</sub> and H<sub>2</sub>O, were computed as well:



Gibbs free energies for the gas-phase species were determined by combining electronic and zero point DFT-PBE energies with experimental enthalpy and entropy corrections [52]. Partial pressures of 4.4, 8.9 and 6.7 bar were used for CO, H<sub>2</sub> and H<sub>2</sub>O, respectively, corresponding to an average CO conversion of 60%. For chemisorbed species, only the electronic energy was included in the calculation of the Gibbs free energy. The experimental thermodynamic data used to evaluate the Gibbs free energy of reaction are provided in Table 2 of the Supplementary material.

To allow comparison with the XPS data, C 1s core-level binding energies were calculated for various carbon species using the final state approximation procedure described by Köhler and Kresse [53]. The accuracy of the calculated core-level binding energies has been estimated to be 20–50 meV [53].

### 3. Results and discussion

In this section, we first present an experimental study of the deactivation behavior of a Co/γ-Al<sub>2</sub>O<sub>3</sub> catalyst during FTS. The catalyst was characterized after 200 h of reaction using a variety of techniques to evaluate the presence and the nature of the deposited carbon species. Next, we calculate the relative stability of various carbon species at terrace sites and near-step edges under Fischer–Tropsch conditions using DFT-PBE. In particular, diffusion into the step sites forming a p4g surface carbide and growth of graphene sheets out of the steps are considered in detail.

#### 3.1. Deactivation behavior and characterization of supported Co catalysts

The FTS activity of a 20 wt% Co/γ-Al<sub>2</sub>O<sub>3</sub> catalyst at 240 °C was evaluated in a fixed-bed micro-reactor for 200 h (Fig. 1). During the first 24 h, the CO conversion increased from about 60% to a maximum of 96%, followed by a gradual loss in activity due to catalyst deactivation. The initial increase in the activity might be due to a further reduction and/or a surface reconstruction of the Co catalysts under syngas conditions [2,20–22]. Both a rapid and a slower deactivation phase were observed, as also reported by others [14,15]. After 200 h on stream, the CO conversion had decreased from a maximum of 96% to 67%. The maximum and final activity, selectivity and particle size are summarized in Table 1. The maxi-

**Table 1**  
Activity, selectivity, chain growth probability, particle size and dispersion for a 20 wt% Co/γ-Al<sub>2</sub>O<sub>3</sub> FTS catalyst. Reaction conditions: 240 °C, 20 bar, H<sub>2</sub>:CO = 2.0, W/F = 7.5 g<sub>cat</sub> h/mol.

	After 25 h	After 200 h
CO conversion (%)	96	67
Turnover frequency <sup>a</sup>	$37 \times 10^{-3}$	$25 \times 10^{-3}$
<i>Hydrocarbon selectivity</i>		
C <sub>1</sub>	24	19
C <sub>2–4</sub>	16	17
C <sub>5+</sub>	60	64
α	0.70	0.72
	Before reaction	After 200 h on stream
Particle size (nm)	10.5 <sup>a</sup>	12.1 <sup>b</sup>
Dispersion (%)	9.5 <sup>a</sup>	8.0 <sup>b</sup>

<sup>a</sup> Based on the number active sites determined by hydrogen chemisorption and averaged over the reactor.

<sup>b</sup> Determined by hydrogen chemisorption after carbon removal by hydrogenation at 500 °C for 2 h.

mum TOF of  $37 \times 10^{-3} \text{ s}^{-1}$  for our 20 wt% Co/γ-Al<sub>2</sub>O<sub>3</sub> catalyst can be compared with the TOFs reported in a review by Ribeiro et al. [54]. Using the power law kinetic model proposed by Ribeiro et al., the TOF reported for a 15 wt% Co/γ-Al<sub>2</sub>O<sub>3</sub> catalyst at 215 °C and 8.2 bar can be extrapolated to a value of  $25 \times 10^{-3} \text{ s}^{-1}$  for our reaction conditions [54]. Our chain growth probability (α) of 0.70 is slightly lower than a value of 0.76 reported by Oukaci et al. for a commercial 20 wt% Co/γ-Al<sub>2</sub>O<sub>3</sub> catalyst operated in a fixed-bed reactor at 220 °C [55].

The methane selectivity is slightly high at 24% but consistent with a temperature of 240 °C. The CO conversion decreased rapidly from 96% to about 80% over the first 50 h. After 50 h, the deactivation rate becomes slower. The selectivity remains relatively unaffected by the catalyst deactivation, with an increase of the C<sub>5+</sub> selectivity from 60% to 64% after 200 h. Overall, the deactivation behavior during the slower phase can be described by a first-order deactivation rate coefficient of  $-1.7 \times 10^{-3} \text{ h}^{-1}$ . The decrease in activity from 96% to 67% over 200 h is comparable to the activity loss reported for a Co/γ-Al<sub>2</sub>O<sub>3</sub> catalyst in a 100 barrels/day slurry bubble column reactor at 230 °C after 200 h [2].

The Co particle size and dispersion were evaluated before and after reaction using H<sub>2</sub> chemisorption experiments (Table 1). To remove deposited carbon species after reaction, the catalysts were hydrogenated at 500 °C for 2 h under 50 N ml/min H<sub>2</sub> before collecting the H<sub>2</sub> adsorption isotherms. A slight decrease in the dispersion from 9.5% to 8.0% was observed after reaction. However, TGA and TPH (Fig. 3) indicate that hydrogenation at 500 °C might not be sufficient to completely remove all the deposited carbon. Therefore, the lower dispersion can, at least in part, be attributed to the incomplete removal of the deposited carbon. TGA indeed indicates that approximately 0.4 mg carbon/g catalyst remains on the Co catalyst after hydrogenation at 500 °C. The equivalent carbon coverage is approximately 0.1 ML and is consistent with a 10% decrease in the dispersion. This value is also comparable to the equivalent carbon coverage of 0.07 ML determined from the TPH profile. Although higher hydrogenation temperatures would further remove these resilient carbon species, unfortunately, they might also lead to sintering of the Co particles [13].

To characterize the nature and the amount of deposited carbon, the deactivated catalyst was studied using a variety of techniques. Based on their reactivity towards hydrogen, different types of deposited carbon can be identified and quantified by deconvolution of the TPH profile (Fig. 3). The sharp peak at 245 °C can be assigned to hydrocarbon wax remaining after extraction with hexane [56]. The equivalent carbon coverage for this peak is 0.12 ML. Most of the resilient carbon corresponds to the broader peaks around 275 and 320 °C with an equivalent coverage of 1.27 ML. The lower

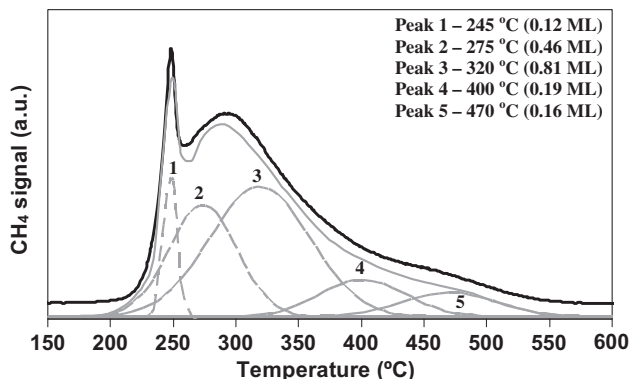


**Fig. 3.** TPH profile for a 20 wt% Co/γ-Al<sub>2</sub>O<sub>3</sub> catalyst after 200 h on stream. The experimental profile (–) was deconvoluted using Gaussian profiles (---). The average temperature and corresponding coverage for each peak are indicated.

temperature peak has been assigned to a surface carbide phase [23], while the higher temperature peak has been attributed to a bulk carbide phase [57]. However, the higher temperature peak at 320 °C has also been attributed to recalcitrant waxes remaining inside the pores of the catalyst [58]. Methane that elutes above 400 °C has been attributed to amorphous and polymeric carbon species [23].

Though the temperature at which the different types of deposited carbon species are hydrogenated is kinetically determined, a relationship with their relative stability can be expected. In the DFT-PBE calculations reported in the next section, three types of adsorbed carbon species were considered, i.e. surface CH<sub>2</sub> and CH groups, a p4g surface carbide phase and extended graphene islands. DFT-PBE calculations indicate that graphene islands are about 20 kJ/mol more stable than a p4g surface carbide phase, and about 50 kJ/mol more stable than surface CH groups. Using a Redhead-type analysis [59], these stability differences can be converted to temperature shifts of approximately 100 °C and 250 °C, corresponding reasonably well with the temperature difference between peak 5, 470 °C, peaks 3 and 4, at 320 and 400 °C, and peak 1, around 245 °C, respectively.

To further characterize the carbon remaining on the catalyst surface after FTS, C 1s XPS spectra were collected for the catalyst after 200 h of reaction and after wax extraction using hexane (Fig. 4). Based on the C 1s binding energies, two forms of resilient carbon with C 1s binding energies of 283.0 and 284.6 eV can be identified. The lower intensity peak at 283.0 eV has been attributed to a Co carbide phase [21], while the broader, higher intensity peak at 284.6 eV can be assigned to a combination of amorphous and polyaromatic species [60,61]. For reference, the C 1s XPS spectrum for the calcined catalyst is included. XPS peaks corresponding to carbidic species have been reported by Xiong et al. [62] for Co/γ-Al<sub>2</sub>O<sub>3</sub> catalysts after 75 h of FTS at 230 °C and 25 bar. In the same study, a Co<sub>2</sub>C phase was detected using XRD. Bulk Co<sub>2</sub>C could not be detected using XRD by Moodley et al. for similar reaction conditions [12]. However, the corresponding TPH data suggest the presence of a surface carbide phase, as well as more resilient carbon species that only hydrogenate above 500 °C. To support the peak assignments, the C 1s core-level binding energies were computed using DFT-PBE. For an extended graphene overlayer on Co(1 1 1), a C 1s core-level binding energy of 284.5 eV was computed, in rea-

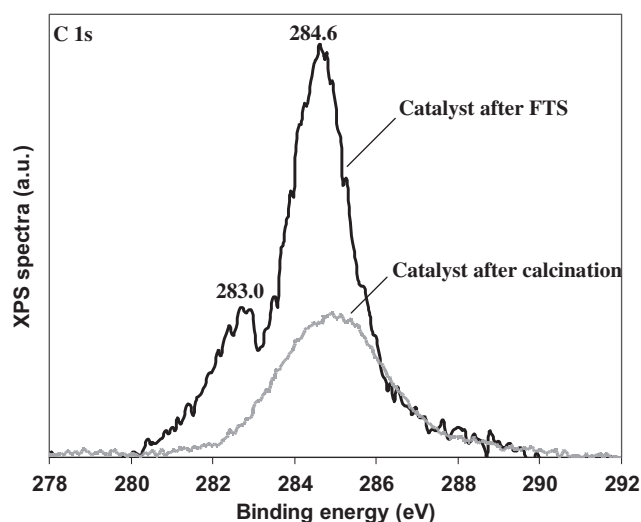


**Fig. 4.** C 1s XPS spectra for a 20 wt% Co/γ-Al<sub>2</sub>O<sub>3</sub> catalyst, after calcination in air (–) and after 200 h of FTS (—). The peak around 284.6 eV can be attributed to a combination of amorphous and polyaromatic carbon species, while the peak around 283.0 eV corresponds to a Co carbide phase.

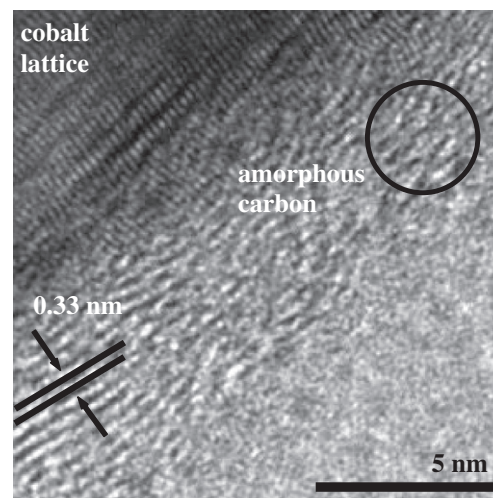


**Fig. 5.** Selected HRTEM image for a 20 wt% Co/γ-Al<sub>2</sub>O<sub>3</sub> catalyst after 200 h of FTS, indicating the presence of both amorphous and polyaromatic-like carbon.

sonable agreement with the broad XPS peak around 284.6 eV. For the p4g surface carbide with 4 rows of carbon per unit cell, a core-level binding energy of 283.4 eV was computed, 1.1 eV weaker than for graphene. Both the absolute value and the shift relative to graphene match the XPS spectra quite well. The core-level binding energy for the p4g surface carbide, 283.4 eV, can further be compared with an experimental binding energy of 283.2 eV reported for a well-characterized p4g surface carbide on a Ni(1 0 0) surface [63]. To evaluate the presence of other types of carbon, C 1s core-level binding energies were also computed for CH<sub>2</sub> on Co(1 1 1) and for a carbon atom in the octahedral sites of the second subsurface layer. The C 1s binding energy of 284.8 eV for surface CH<sub>2</sub> is stronger than for graphene and cannot explain the

**Table 2**

Binding energies and Gibbs free energies of reaction, ΔG<sub>r</sub> (500 K, 20 bar), under FTS conditions for carbon and CH<sub>x</sub> adsorption on the Co(1 1 1) surface at 0.25 ML.

Species	Binding energy/ΔG <sub>r</sub> <sup>a</sup> (kJ/mol C)
<i>Carbon</i>	
On-surface (hcp hollow)	–658/–4
Subsurface (octahedral)	–660/–6
<i>CH</i>	
On-surface (hcp hollow)	–610/–18
<i>CH<sub>2</sub></i>	
On-surface (hcp hollow)	–400/–17
<i>Graphene<sup>b</sup></i>	
Carbon at fcc hollow and atop site	–769/–115
Carbon at bridge and near atop site	–770/–116

<sup>a</sup> Gibbs free energy of reaction for CO (g) + (x/2 + 1) H<sub>2</sub> (g) ↔ CH<sub>x</sub> + H<sub>2</sub>O (g).

<sup>b</sup> Carbon coverage of 2.0 ML.

**Table 3**

Carbon binding energy and Gibbs free energy of reaction, ΔG<sub>r</sub> (500 K, 20 bar), under FTS conditions on a stepped Co surface (Fig. 1).

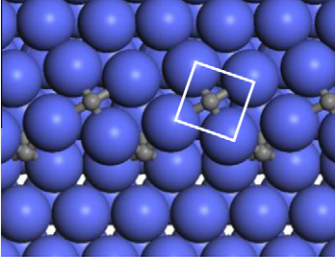
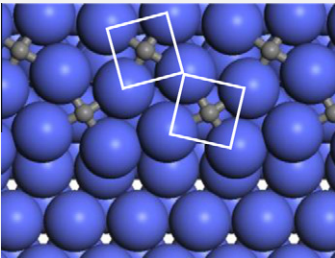
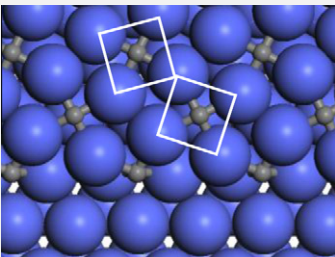
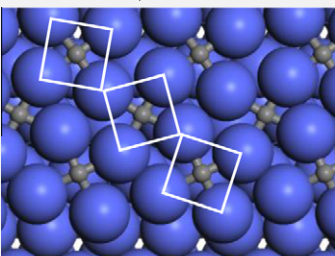
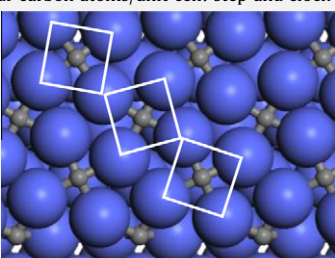
Adsorption site	Binding energy/ΔG <sub>r</sub> <sup>a</sup> (kJ/mol carbon)	
	p(4 × 8) unit cell	p(2 × 8) unit cell
Step site (S)	–747/–93	–715/–61
Subsurface (Sub)		–652/+2
p4g clock reconstruction (E1)	–662/–8 <sup>b</sup>	–697/–43
Fcc hollow near edge (E2)		–653/+1

<sup>a</sup> Gibbs free energy for CO (g) + (x/2 + 1) H<sub>2</sub> (g) ↔ CH<sub>x</sub> + H<sub>2</sub>O (g) (Eq. (2)).

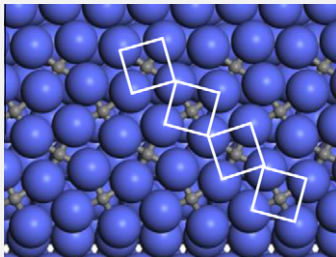
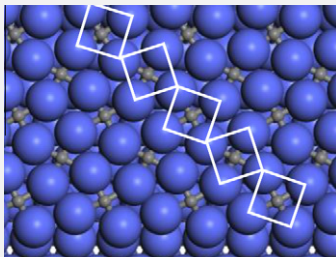
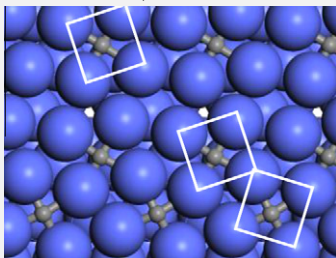
<sup>b</sup> No reconstruction was observed at lower step coverages.

experimental peak at 283.0 eV. Experimentally, a C 1s binding energy of 284.9 eV has been reported for  $\text{CH}_2$  groups on Co [64]. The DFT-PBE C 1s core-level binding energy for subsurface carbon is

**Table 4**  
Carbon binding energies and Gibbs free energies of reaction,  $\Delta G_r$  (500 K, 20 bar), under FTS conditions for carbon adsorption at step sites and for a p4g clock surface carbide on a stepped Co surface. Squares are used to indicate p4g clock sites.

Adsorption structure	Binding energy/ $\Delta G_r^a$ (kJ/mol C)
Two carbon atoms/unit cell: step and clock	-734/-80
	
Two carbon atoms/unit cell: clock	-746/-92
	
Three carbon atoms/unit cell: step and clock	-738/-84
	
Three carbon atoms/unit cell: clock	-750/-96
	
Four carbon atoms/unit cell: step and clock	-743/-89
	

**Table 4** (continued)

Adsorption structure	Binding energy/ $\Delta G_r^a$ (kJ/mol C)
Four carbon atoms/unit cell: clock	-751/-97 <sup>b</sup>
	
Five carbon atoms/unit cell: clock	-752/-98 <sup>b</sup>
	
Three carbon atoms/unit cell: rows 1, 2 and 4	-738/-84 <sup>b</sup>
	

<sup>a</sup> Gibbs free energy for the  $\text{CO}(\text{g}) + (x/2 + 1) \text{H}_2(\text{g}) \leftrightarrow \text{CH}_x + \text{H}_2\text{O}(\text{g})$  (Eq. (2)) reaction under FTS conditions.

<sup>b</sup> Modeled with a  $p(2 \times 8)$  unit cell with two upper rows of Co atoms removed.

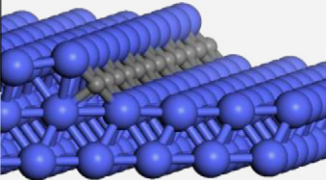
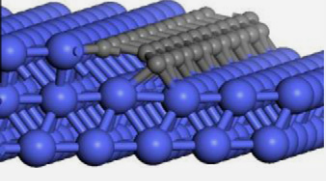
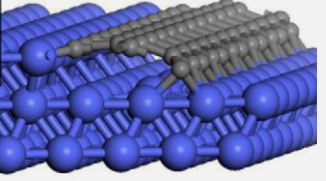
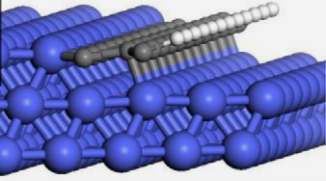
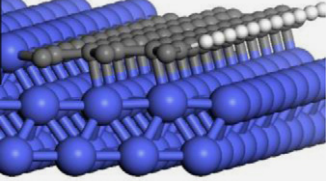
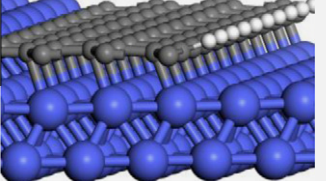
283.9 eV, intermediate between the value for graphene and for a p4g surface carbide.

To visualize the carbon deposits on the catalyst surface, the Co catalysts were studied with HRTEM, again after extraction of the hydrocarbon waxes. The image in Fig. 5 shows the presence of lamellar carbon deposits with an interlayer spacing of about 0.33 nm, similar to the interlayer spacing in graphite [65]. However, unlike graphitic carbon, the structure is not perfectly ordered. At the fringes of the lamellar carbon, irregular amorphous carbon deposits can be seen as well. Previous HRTEM studies of Co/ $\gamma$ - $\text{Al}_2\text{O}_3$  catalysts after FTS in a slurry bubble column reactor at somewhat lower temperature and lower CO conversion only reported the presence of amorphous carbon deposits, though the corresponding TPH characterization did indicate the presence of more resilient carbon species [12].

### 3.2. Computational evaluation of the relative stability of various forms of deposited carbon

In this section, DFT-PBE calculations are reported to evaluate the stability of different carbon species under FTS reaction conditions. First, the stability of C, CH and  $\text{CH}_2$  species on the Co(1 1 1) terraces are calculated (Table 2). Next, the stability of atomic carbon, of a p4g surface carbide, and of graphene islands on a model stepped surface are evaluated (Table 3). The preferred on-surface adsorption site for C, CH and  $\text{CH}_2$  species on the Co(1 1 1) terraces

**Table 5**  
Carbon binding energies and Gibbs free energies of reaction,  $\Delta G_r$  (500 K, 20 bar), under FTS conditions for the evolution of graphene strips on a stepped Co surface.

Adsorption structure	Binding energy/ $\Delta G_r^a$ (kJ/mol C)
One row of carbon atoms 	–660/–6
Three row of carbon atoms 	–686/–32
Five rows of carbon atoms 	–702/–48
Three rows of carbon atoms, hydrogen terminated 	n.a./–76
Five rows of carbon atoms, hydrogen terminated 	n.a./–80
Seven rows of carbon atoms, hydrogen terminated 	n.a./–82 <sup>b</sup>

<sup>a</sup> Gibbs free energy for the  $\text{CO}(\text{g}) + (x/2 + 1) \text{H}_2(\text{g}) \leftrightarrow \text{CH}_x + \text{H}_2\text{O}(\text{g})$  reaction under FTS conditions.

<sup>b</sup> Modeled with  $p(2 \times 8)$  unit cell with five upper rows of Co atoms removed.

is calculated to be the hcp hollow site, consistent with the literature [24,66]. Also, the calculated binding energies of  $-658$ ,  $-610$  and  $-400$  kJ/mol, respectively, are comparable to literature values [24,66]. Carbon at the subsurface octahedral sites is only 2 kJ/mol more stable than surface carbon, and there is no strong driving force for carbon to diffuse to the subsurface sites. The proposed FTS intermediates  $\text{CH}^*$  and  $\text{CH}_2^*$  are thermodynamically stable under FTS conditions, and more stable than both surface and subsurface carbon.  $\text{CH}^*$  and  $\text{CH}_2^*$  species can undergo C–C coupling to further gain stability [26]. The most stable carbon form on Co(1 1 1) terraces is found to be graphene. Four high symmetry orientations were considered for the graphene overlayers, and all have a comparable stability. The two most stable structures are included in Table 2. The other structures are 5 and 9 kJ/mol carbon less stable. Most of the carbon binding energy in graphene results from the strong carbon–carbon bonds, with a calculated gas-phase binding energy of  $-768$  kJ/mol. The interaction energy of a graphene sheet with the Co(1 1 1) surface is quite weak at  $0.015$  J/m<sup>2</sup>. This value can be compared with an interaction energy of  $0.023$  J/m<sup>2</sup> reported in a recent Van der Waals DFT study that includes nonlocal dispersion interactions [67].

Next, the stability of carbon on a stepped Co surface was evaluated (Fig. 2 and Table 3). The binding energy at the hollow fcc site on the lower terrace of this surface (H) is  $-650$  kJ/mol, similar to the  $-658$  kJ/mol on the Co(1 1 1) terrace (Table 2). Also, the binding energy at the fcc site near the step edge (E2) and at the subsurface octahedral sites (Sub) are comparable to the values determined for the Co(1 1 1) surface. The most stable adsorption site on the stepped surface is the step site (S) with a binding energy of  $-715$  kJ/mol for a step coverage of 50% and  $-747$  kJ/mol for a coverage of 25%. Carbon at the near-edge hcp hollow site (E1) does not remain above the surface, but sinks into the Co surface and initiates a p4g type clock reconstruction of the (1 1 1) facet, as illustrated in Table 4. The optimized structure resembles the structure determined by LEED for carbon adsorption on Ni(1 0 0), with the carbon atom located approximately 0.1 Å above the surface [36]. The reconstruction is driven by the enhanced carbon binding energy at the E1 site. Indeed, the energy cost to reconstruct the step edge to a clock-like structure is approximately 64 kJ/mol. This energy cost is more than compensated by the 115 kJ/mol increase in the carbon binding energy at the new 4-fold hollow sites. A critical carbon surface concentration of 0.5 ML has been reported to initiate a p4g clock reconstruction on Ni(1 0 0) [68]. Also on the stepped Co(1 1 1) model surface, a high step coverage is required to stabilize the p4g reconstruction (Table 2).

The calculations reported in Tables 2 and 3 indicate that extended graphene islands, carbon at step sites and a p4g surface carbide are thermodynamically stable under typical FTS conditions with Gibbs free energies of reaction of  $-116$ ,  $-61$  and  $-43$  kJ/mol, respectively. Experimental XPS and HRTEM data reported in Figs. 4 and 5 further indicate the presence of a polyaromatic phase and of a surface carbide phase after FTS. Since both graphene islands and a p4g clock reconstruction are found to nucleate from step sites on a stepped Ni surface [28–30,35,37,38], we next consider the stability of an extended p4g surface carbide (Table 4) and of graphene strips (Table 5) for a stepped Co surface.

Various combinations of carbon at the p4g clock sites and at the step sites were considered; only the most stable structures are summarized in Table 4. The calculations indicate that the formation of an extended p4g surface carbide is highly favorable with a converged binding energy of about  $-750$  kJ/mol. While the average Gibbs free energy to form a single row of p4g surface carbide near the step edge is  $-43$  kJ/mol (Table 3), the driving force increases to  $-92$  kJ/mol for two rows and  $-96$  kJ/mol for three rows. To evaluate the convergence of the carbon binding energy, a slab with six Co rows in the top layer of a  $p(2 \times 8)$  unit cell was used.

Computed Gibbs free energies of  $-97$  kJ/mol for four rows and  $-98$  kJ/mol for five rows of carbon indicate that the binding energies are converged. Though carbon adsorption at the step sites is more favorable than a single row of p4g surface carbide, the formation of a second row of p4g surface carbide is 12 kJ/mol more favorable than adsorption at the step sites near the first row of p4g surface carbide (Table 4). A similar preference was computed for three rows of carbon. Note that the p4g clock reconstruction of the step edge also increases the carbon binding energy at the step from  $-715$  kJ/mol (Table 3) to  $-771$  kJ/mol (Table 4), as it did for carbon at the hollow site. The calculations further indicate that the p4g surface carbide favors a row-by-row growth mechanism from the steps. Indeed, occupying the clock sites at rows 1, 2 and 3 is 36 kJ/mol more favorable than occupying rows 1, 2 and 4 (Table 4). This is consistent with the ordered p4g clock reconstruction that grows from step defects on a Ni surface after CO and ethylene decomposition, as observed with STM [37,38].

Instead of diffusing into the step sites to form a surface carbide, carbon atoms can also grow out of the step sites to form graphene islands. In this paragraph, we will discuss the stability of graphene strips of 1, 3, 5 and 7 carbon atoms wide and consider the effect of hydrogen termination on their stability. The DFT-PBE results are summarized in Table 5. Based on our simulations, extended graphene islands are the most stable form of carbon on Co, with a free energy of reaction of  $-116$  kJ/mol under FTS conditions. They are more stable than the extended p4g surface carbide, with a stability of about  $-98$  kJ/mol. However, small islands of graphene are significantly less stable. The formation of graphene islands on a catalyst surface can therefore be described as a typical nucleation and growth process, and step sites have been identified as possible nucleation centers [28–30]. A first set of calculations evaluates the stability of a single row of carbon atoms at the step sites. For a step coverage of 100%, carbon is 87 kJ/mol less stable than for a step coverage of 25%, 86 kJ/mol less stable than two rows of p4g surface carbide, and 109 kJ/mol less stable than extended graphene islands. However, the stability increases as the graphene strips become wider. The first aromatic ring can be closed for three rows of carbon, and the stability becomes  $-32$  kJ/mol. For five rows of carbon, the second ring can be closed, and the average stability reaches  $-48$  kJ/mol. This is still significantly less stable than an equivalent island of p4g surface carbide. The low stability of the graphene strips can be attributed to the unsaturated edge sites [28,32]. To reduce the unsaturation of the edge sites and gain stability, the graphene strips typically form arch-like structures (Table 5). However, an alternative way to reduce the unsaturation of the edge carbon atoms is by hydrogenation. To evaluate this option, we calculated the stability of hydrogen-terminated graphene strips, again using Eq. (2). Hydrogen termination enhances the stability of graphene strips by 44 kJ/mol carbon for three rows of carbon and by 32 kJ/mol carbon for five rows. Moreover, hydrogen termination causes the graphene strips to become parallel to the Co surface, with an average graphene to surface distance of about 2.1 Å, similar to the distance of 2.0 Å for an infinite layer of graphene on Co(1 1 1). However, even after hydrogen termination, the 3, 5 and 7 carbon atom-wide graphene strips remain about 15 kJ/mol carbon less stable than the extended p4g surface carbide.

#### 4. Conclusions

Supported 20 wt% Co/ $\gamma$ -Al<sub>2</sub>O<sub>3</sub> FTS catalysts were tested in a fixed-bed micro-reactor for 200 h at 240 °C and 20 bar. Over this period, the catalyst lost 30% of its maximum FTS activity with a first-order deactivation coefficient of  $-1.7 \times 10^{-3}$  h<sup>-1</sup>. Post-reaction characterization indicates that two types of resilient carbon species have formed on the catalyst. C 1s XPS spectra suggest that



a surface carbide phase and a polyaromatic carbon phase remain on the catalyst after wax extraction. The C 1s binding energies of 283.0 and 284.6 eV compare well with DFT-PBE calculated core-level binding energies of 283.4 eV for a surface p4g carbide phase and 284.5 eV for extended graphene islands. HRTEM images further confirm the presence of lamellar carbon species on the catalyst after reaction. The stability of various carbon species under reaction conditions was evaluated using DFT-PBE. Extended graphene islands and a p4g surface carbide were found to be 99 and 79 kJ/mol more stable than surface CH<sub>2</sub> groups. Both carbon phases initiate and grow from step sites. Carbon atoms can diffuse into the step sites to form the p4g surface carbide or grow out of the steps to form graphene strips. Though extended graphene islands are very stable, small graphene strips are significantly less stable due to the unsaturated edge sites. Hydrogen termination of the edge carbon atoms enhances the stability of the graphene strips, but even a hydrogen-terminated, 8-Å-wide graphene strip remains 15 kJ/mol carbon less stable than an equivalent, 14-Å-wide surface p4g carbide phase.

### Acknowledgments

Financial and experimental support from the Agency for Science, Technology and Research (A-Star project 062-101-0035) and from the National University of Singapore are gratefully acknowledged.

### Appendix A. Supplementary material

Supplementary data associated with this article can be found, in the online version, at doi:10.1016/j.jcat.2010.06.008.

### References

- [1] J.P. Collins, J.J.H.M. Font Freide, B. Nay, *J. Nat. Gas. Chem.* 15 (2006) 1.
- [2] A.M. Saib, A. Borgna, J. van de Loosdrecht, P.J. van Berge, J.W. Niemantsverdriet, *Appl. Catal. A* 312 (2006) 12.
- [3] A.M. Saib, A. Borgna, J. van de Loosdrecht, P.J. van Berge, J.W. Niemantsverdriet, *J. Phys. Chem. B* 110 (2006) 8657.
- [4] E. Iglesia, *Appl. Catal. A* 161 (1997) 59.
- [5] B.H. Davis, *Ind. Eng. Chem. Res.* 46 (2007) 8938.
- [6] A.M. Saib, D.J. Moodley, I.M. Ciobîcă, M.M. Hauman, B.H. Sigwebela, C.J. Weststrate, J.W. Niemantsverdriet, J. Van de Loosdrecht, *Catal. Today* (2010), doi:10.1016/j.cattod.2010.02.008.
- [7] N.E. Tsakoumis, M. Rønning, Ø. Borg, E. Rytter, A. Holmen, *Catal. Today* (2010), doi:10.1016/j.cattod.2010.02.077.
- [8] D. Schanke, A.M. Hilmen, E. Bergene, K. Kinnari, E. Rytter, E. Ådnanes, A. Holmen, *Catal. Lett.* 34 (1995) 269.
- [9] G. Jacobs, P.M. Patterson, Y. Zhang, T. Das, J. Li, B.H. Davis, *Appl. Catal. A* 233 (2002) 215.
- [10] G. Jacobs, P.M. Patterson, T.K. Das, M. Luo, B.H. Davis, *Appl. Catal. A* 270 (2004) 65.
- [11] O. Ducreux, J. Lynch, B. Rebours, M. Roy, P. Chaumette, *Stud. Surf. Sci. Catal.* 119 (1998) 125.
- [12] D.J. Moodley, J. van de Loosdrecht, A.M. Saib, M.J. Overett, A.K. Datye, J.W. Niemantsverdriet, *Appl. Catal. A* 354 (2009) 102.
- [13] J.J.H.M. Font Freide, T.D. Gamlin, R.J. Hensman, B. Nay, C. Sharp, *J. Nat. Gas Chem.* 13 (2004) 1.
- [14] E. Iglesia, S.L. Soled, R.A. Fiato, G.H. Via, *J. Catal.* 143 (1993) 345.
- [15] P.J. van Berge, R.C. Everson, *Stud. Surf. Sci. Catal.* 107 (1997) 207.
- [16] A. Martínez, J. Rollán, M.A. Arribas, H.S. Cerqueira, A.F. Costa, E.F. S-Aguiar, *J. Catal.* 249 (2007) 162.
- [17] S.L. Soled, E. Iglesia, R.A. Fiato, G.B. Ansell, United States Patent 5397,806, 1995 (to Exxon).
- [18] M.J. van der Burgt, J. Ansorge, Great Britain Patent 2222,531, 1988 (to Shell).
- [19] H.A. Wright, United States Patent 6486,220 B1, 2002 (to Conoco).
- [20] G.A. Beitel, C.P.M. de Groot, H. Oosterbeek, J.H. Wilson, *J. Phys. Chem. B* 101 (1997) 4035.
- [21] G.A. Beitel, A. Laskov, H. Oosterbeek, E.W. Kuipers, *J. Phys. Chem.* 100 (1996) 12494.
- [22] J. Wilson, C. de Groot, *J. Phys. Chem.* 99 (1995) 7860.
- [23] D.-K. Lee, J.-H. Lee, S.-K. Ihm, *Appl. Catal.* 36 (1988) 199.
- [24] D.J. Klinke, S. Wilke, L.J. Broadbelt, *J. Catal.* 178 (1998) 540.
- [25] J.C.W. Swart, E. van Steen, I.M. Ciobîcă, R. A van Santen, *Phys. Chem. Chem. Phys.* 11 (2009) 803.
- [26] J.C.W. Swart, I.M. Ciobîcă, R. A van Santen, E. van Steen, *J. Phys. Chem. C* 112 (2008) 12899.
- [27] I.M. Ciobîcă, R.A. van Santen, P.J. van Berge, J. van de Loosdrecht, *Surf. Sci.* 602 (2008) 17.
- [28] H.S. Beengard, J.K. Nørskov, J. Sehested, B.S. Clausen, L.P. Nielsen, A.M. Molenbroek, J.R. Rostrup-Nielsen, *J. Catal.* 209 (2002) 365.
- [29] F. Besenbacher, I. Chorkendorff, B.S. Clausen, B. Hammer, A.M. Molenbroek, J.K. Nørskov, I. Stensgaard, *Science* 279 (1998) 1913.
- [30] H.S. Bengaard, I. Alstrup, I. Chorkendorff, S. Ullmann, J.R. Rostrup-Nielsen, J.K. Nørskov, *J. Catal.* 187 (1999) 238.
- [31] J.R. Rostrup-Nielsen, *J. Catal.* 85 (1984) 31.
- [32] J. Xu, M. Saeys, *J. Catal.* 242 (2006) 217.
- [33] J. Xu, L. Chen, K.F. Tan, A. Borgna, M. Saeys, *J. Catal.* 261 (2009) 158.
- [34] J. Xu, M. Saeys, *J. Phys. Chem. C* 113 (2009) 4099.
- [35] M.P. Andersson, F. Abild-Pedersen, *Surf. Sci.* 601 (2007) 649.
- [36] J.H. Onuferko, D. P Woodruff, B.W. Holland, *Surf. Sci.* 87 (1979) 357.
- [37] H. Nakano, J. Nakamura, *Surf. Sci.* 482 (2001) 341.
- [38] R.T. Vang, K. Honkala, S. Dahl, E.K. Vestergaard, J. Schnadt, E. Lægsgaard, B.S. Clausen, J.K. Nørskov, F. Besenbacher, *Surf. Sci.* 600 (2006) 66.
- [39] G.F. Froment, K.B. Bischoff, *Chemical Reactor Analysis and Design*, second ed., John Wiley & Sons, New York, 1990. p. 166.
- [40] Y. Zhang, Y. Liu, G. Yang, S. Sun, N. Tsubaki, *Appl. Catal. A* 321 (2007) 79.
- [41] N. Tsubaki, S. Sun, K. Fujimoto, *J. Catal.* 199 (2001) 236.
- [42] G.V. Pankina, P.A. Chernavskii, A.S. Lermontov, V.V. Lunin, *Petrol. Chem.* 42 (2002) 217.
- [43] J. Li, N.J. Coville, *Appl. Catal. A* 208 (2001) 177.
- [44] J. Li, N.J. Coville, *Appl. Catal. A* 181 (1999) 201.
- [45] Ø. Borg, S. Eri, E.A. Blekkan, S. Storsæter, H. Wigum, E. Rytter, A. Holmen, *J. Catal.* 248 (2007) 89.
- [46] S. Storsæter, Ø. Borg, E.A. Blekkan, A. Holmen, *J. Catal.* 231 (2005) 405.
- [47] J.P. Perdew, K. Burke, M. Ernzerhof, *Phys. Rev. Lett.* 77 (1996) 3865.
- [48] G. Kresse, J. Hafner, *Phys. Rev. B* 47 (1993) 558.
- [49] G. Kresse, J. Hafner, *Phys. Rev. B* 48 (1993) 13115.
- [50] E. van Steen, M. Claeys, M.E. Dry, J. van de Loosdrecht, E.L. Viljoen, J. L Visagie, *J. Phys. Chem. B* 109 (2005) 3575.
- [51] N.W. Ashcroft, N.D. Mermin, *Solid State Physics*, Holt, Rinehart and Winston, New York, 1976. p. 70.
- [52] M.W. Chase, *J. Phys. Chem. Ref. Data, Monograph* 9 (1998) 1.
- [53] L. Köhler, G. Kresse, *Phys. Rev. B* 70 (2004) 165405.
- [54] F.H. Ribeiro, A.E. Schach von Wittenau, C.H. Bartholomew, G.A. Somorjai, *Catal. Rev. Sci. Eng.* 39 (1997) 49.
- [55] R. Oukaci, A.H. Singleton, J.G. Goodwin, *Appl. Catal. A* 186 (1999) 129.
- [56] V. Gruver, R. Young, J. Engman, H.J. Robota, *Prep. Pap. Am. Chem. Soc. Div. Petrol. Chem.* 50 (2005) 164.
- [57] J. Xu, C.H. Bartholomew, *J. Phys. Chem. B* 109 (2005) 2392.
- [58] V. Gruver, X. Zhan, J. Engman, H.J. Robota, *Prep. Pap. Am. Chem. Soc. Div. Petrol. Chem.* 49 (2004) 192.
- [59] P.A. Redhead, *Vacuum* 12 (1962) 203.
- [60] J.F. Moulder, *Handbook of X-ray Photoelectron Spectroscopy*, Perkin Elmer, Eden Prairie, 1982. p. 147.
- [61] F. Le Normand, J. Hommet, T. Szörénti, C. Fuchs, E. Fogarassy, *Phys. Rev. B* 64 (2001) 235416.
- [62] J. Xiong, Y. Ding, T. Wang, L. Yan, W. Chen, H. Zhu, Y. Lu, *Catal. Lett.* 102 (2005) 265.
- [63] N. Mårtensson, A. Nilsson, *J. Electron Spectrosc. Relat. Phenom.* 75 (1995) 209.
- [64] F. Solymosi, I. Kovács, *Surf. Sci.* 296 (1993) 171.
- [65] D. Tománek, S.G. Louie, *Phys. Rev. B* 37 (1988) 8327.
- [66] X.-Q. Gong, R. Raval, P. Hu, *J. Chem. Phys.* 122 (2005) 024711.
- [67] M. Vanin, J.J. Mortensen, A.K. Kelkkanen, J.M. Garcia-Lastra, K.S. Thygesen, K.W. Jacobsen, *Phys. Rev. B* 81 (2010) 081408.
- [68] C. Klink, L. Olesen, F. Besenbacher, I. Stensgaard, E. Lægsgaard, N.D. Lang, *Phys. Rev. Lett.* 71 (1993) 4350.